SSRG International Journal of Electronics and Communication Engineering
ISSN: 2348-8549/ https://doi.org/10.14445/23488549/IJECE-V12I11P108

Voume 12 Issue 11, 103-114, November 2025

Original Article

A Photonic Radar Aided DCNN-Based Classification of LSS Targets Using their ISAR-Images: DIAT-ISAR-sATIs

Nargis Akhter[1], Ajay Waghumbare[2], A. Arockia Bazil Raj[3]

[1]*RF Photonics Laboratory, Defence Institute of Advanced Technology (DIAT), Pune, India.*
[2]*School of Computer Engineering and Mathematical Sciences, Defence Institute of Advanced Technology (DIAT), Girinagar, Pune, India.*
[3]*RF Photonics Laboratory, Defence Institute of Advanced Technology (DIAT), Pune, India.*

[3]*Corresponding Author : brazilraj.a@diat.ac.in*

Received: 08 September 2025 Revised: 10 October 2025 Accepted: 09 November 2025 Published: 29 November 2025

Abstract *- Protective measures for national, military, or civil surveillance systems are critical for the automatic detection and identification of various aerial Low-altitude Slow-speed Smaller size (LSS) targets accurately. In this study, a diversified "Defense Institute of Advanced Technology-Inverse Synthetic Aperture Radar-small Aerial Target Images (DIAT-ISAR-sATIs)" dataset consisting of 4320 Inverse Synthetic Aperture Radar (ISAR) images of five distinct aerial LSS targets is constructed using an ultra-broadband (6-12 GHz Instantaneous Bandwidth (IBW)) Stepped Frequency Modulated Continuous Wave (SFMCW) photonic radar. After data augmentation, the dataset was increased to 6000 samples. Additionally, a Deep Convolutional Neural Network (DCNN) approach based on transfer learning was introduced for the classification of aerial LSS targets. The method achieved a classification accuracy of 98.67% on validation samples and 95.56% on open-field samples by utilizing a pretrained MobileNetV2 as the feature extractor, with minimal occurrences of false negatives and false positives. The experimental classes investigated in this study are 1) an RC plane; 2) a mini-helicopter; 3) a DJIF 450; 4) a Scythe 4s racer; 5) a bionic-bird; and 6) a combination of a mini-helicopter and a bionic-bird. Experimental results demonstrate that the proposed pre-trained DCNN model outperforms existing pre-trained models on the DIAT-ISAR-sATIs dataset.*

Keywords *- Photonic radar, Inverse synthetic aperture radar imaging, Low-altitude slow-speed smaller-size targets, Deep convolutional neural network.*

1. Introduction

Microwave-photonics technology [1] is replacing the traditional RF transportation technologies such as radio over fiber, radar, and Electronic Warfare (EW) due to its superior benefits [2], including low timing/phase jitter, ultra-wide instantaneous bandwidth, photonic signal processing, Electromagnetic Interference (EMI) immunity, compact size, and minimal transmission loss. Therefore, effective situational assessment in military/civilian surveillance critically depends on high-performance Automatic Target Detection (ATD) utilizing the range-Doppler (r-D) & micro-Doppler (m-D) signatures of aerial Low-altitude Slow-speed Smaller-size (LSS) targets—such as drones, UAVs, quadcopters, mini-helicopters, and bionic devices—now made feasible by photonic-assisted radar systems. Relying solely on r-D/m-D components/images presents a significant challenge when multiple LSS targets hover/move at identical rotational/flapping speeds, causing their r-D/m-D signatures to overlap and complicate detection [1, 3]. At the same time, Inverse Synthetic Aperture Radar (ISAR) offers spatial information, i.e., detailed LSS targets structure-related information in all-day and weather conditions, which supports the accurate detection and classification of LSS targets [4]. Therefore, ISAR-based detection and classification of aerial LSS targets are currently gaining major attention and emerging as a significant focus of extensive research [5].

Traditional ISAR image classification methods typically depend on static features, including target texture, contour, direction, and size [6, 7]. They are noticeably less effective in terms of transferability, correct classification, and feature representation. Recently, deep learning has emerged as a promising approach for ISAR target classification [8]. In [9], the authors introduced a two-stage network for the classification of ISAR target images. They have proposed a Robust Embedding and Manifold Inference (REMI) method that improves classification accuracy. In [10], the authors examine the application of 3D-ISAR for classifying maritime for aspect angles of 0◦, 20◦, 40◦, and 60◦.

Fig. 1 LSS targets: (a)RC plane, (b)mini-helicopter, (c)DJIF 450, (d)Scythe 4s racer, and (e) bionic-bird.

In [11], the paper targets and has achieved a classification accuracy of 99.15% discussing ISAR image enhancement algorithms as well as neural network architecture for image recognition and target identification. Two Learning Vector Quantization (LVQ) neural networks are proposed to perform image recognition of aerial targets (different aircraft). Pretrained CNNs are used to classify micro-Doppler signatures of small aerial targets [12]. They consist of six classes and have achieved a classification accuracy of 97%. In their study [13], Park et al. proposed a ResNet-SP Convolutional Neural Network (CNN) model designed to classify different types of UAVs, including quadcopters, bionic bird-Metafly, and bionic-bird-Disco, using spectrogram images derived from X-band radar signals.

The model achieved a classification accuracy of 83.39%. In [14], authors classified ISAR images of automotive targets (simulated model) such as: auto-rickshaw (tuk-tuk); full-sized car; bicycle; truck; mid-sized car, etc., using transfer learning, have achieved an accuracy of 98%. Most studies indicate that ISAR images show strong potential for recognizing both aerial and ground targets.

From the above literature, it is observed that they have considered only 1) aerial/ground-based targets, 2) large aerial targets, 3) fewer dataset classes, 4) operation of individual target (not combination), and 5) m-D signatures of small aerial vehicles. Today, the operation of various similar aerial LSS targets includes threats such as mini-helicopters, 2-blade and 3-blade propeller systems, high-wing RC planes, fixed-wing UAVs, and bionic birds.

Additionally, the compact size of these aerial LSS targets allows the simultaneous operation of multiple different targets, posing potential threats [15]. For classifying aerial LSS targets, a neural network-based approach is preferable. When assessing the performance of a CNN model, the total number of parameters plays a key role in determining computational complexity. In addition to overall accuracy, metrics such as precision, recall, F1-score, macro average, and weighted average are essential for comprehensively evaluating the model's classification performance [16]. This paper presents the Defense Institute of Advanced Technology–Inverse Synthetic Aperture Radar–small Aerial Target Images (DIAT-ISAR-sATIs) dataset, which consists of 4,320 ISAR images of five aerial LSS, as illustrated in Figure 2, considering real-time scenarios. The dataset was augmented through rotations of 30°, 60°, and horizontal flips, increasing the total number of samples to 6,000.

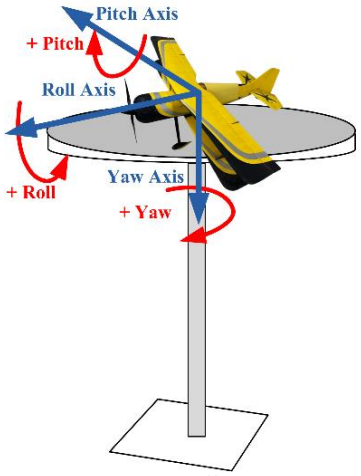

Fig. 2 A LSS target (RC Plane) in Different Pitch/Roll/Yaw rotation axes on the turntable

An ultra-wide instantaneous bandwidth of 6-12 GHz photonics Stepped Frequency Modulated Continuous Wave (SFMCW) radar was developed to detect and classify aerial LSS targets by generating their ISAR images. Additionally, a Deep Convolutional Neural Network (DCNN) model based on transfer learning was introduced to classify these targets using their ISAR images.

A dataset was developed utilizing the photonic SFMCW radar by the simultaneous operation of single and multiple LSS targets to observe a comparative classification accuracy in cases of one or more than one target's existence. The main contributions of this work can be summarized as:

- An ultra-wide instantaneous bandwidth of 6-12 GHz photonic Stepped Frequency Modulated Continuous Wave (SFMCW) radar is developed.
- To enhance the structural visibility and representation of LSS targets in ISAR images, a contour-based noise removal algorithm is introduced prior to classification [17].
- A novel dataset (DIAT-ISAR-sATIs) is developed, consisting of 6000 (ISAR) images of aerial LSS targets generated by utilizing the photonic SFMCW radar.
- The dataset includes individual five single LSS targets operation and one combined operation of two targets with varying aspect angles, geometric orientation, and ranges.

- A fine-tuned MobileNetV2 is proposed for automatic LSS target classification based on their ISAR images.
- The proposed DCNN model achieved 98.67% accuracy on validation data and 95.56% on open-field test data, with minimal false positives and false negatives.
- A comparative evaluation was done to demonstrate the outperformance of the proposed model with other standard pre-trained CNN models on the DIAT-ISAR-sATIs dataset.

The remaining part of the paper is structured as follows: Section 2 discusses the necessity of photonic radar to detect the aerial LSS targets, the in-house-built ultra-broadband photonic SFMCW radar is described in Section 3, and in Section 4, the methodology used to generate the ISAR images is presented.

Section 5 discusses the post-image processing, and Section 6 describes the proposed DCNN model. The results and performance analysis of the proposed model are reported in Section 7, and lastly, a conclusion is provided in Section 8, providing the future scope of the work.

2. Necessity of Photonics Radar Technology

The requirements of high-resolution, high-speed, and interference-resistant systems are increasing day by day in radar technology. To address this demand, photonic radar technology has emerged as an innovative alternative to the traditional electrical radar.

In a traditional radar system, all the electrical components used for RF signal generation, transmission, and processing face lots of challenges due to the high-frequency losses, susceptibility to EMI, and limitations in bandwidth and resolution. However, by integrating the optical components, photonic radar easily overcomes these drawbacks, enabling precise and low-loss RF signal processing.

The RF-photonics technology is the combination of photonics and microwave technologies, which enhances the RF signal generation, transmission, and detection capacity [18]. This approach is highly beneficial for defense systems, automotive sensors, aerospace technologies, and remote sensing. In a photonic radar system, the RF transmissions are done in the optical domain using an Electro-Optical Modulator (EOM). This modulator modulates an optical signal and transmits it through low-noise optical fibers.

Within this optical domain, the signal passes through other optical components, such as optical amplifiers, optical filters, and high-speed photodetectors, which convert the processed optical signal back into RF signals. Thus, the RF-photonics system offers significant benefits, including an ultra-wide bandwidth, superior target resolution, and resistance to electronic jamming. Photonic radar becomes a suitable tool for complex and dynamic operational environments due to its versatility and real-time reconfigurability. As the demand for sophisticated radar systems continues to grow, photonic radar is expected to play a pivotal role in shaping the next generation of high-performance and adaptive radar technologies.

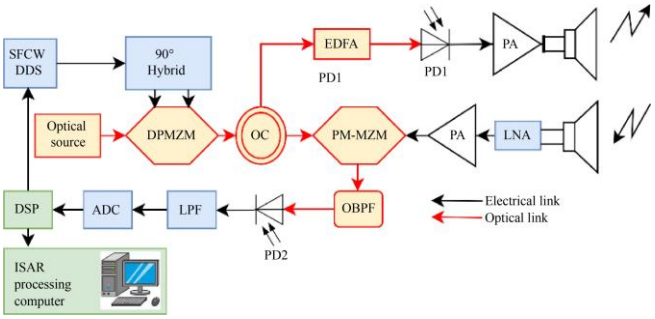

Fig. 3 Top-level schematic of the developed ultra-broadband Photonic SFMCW Radar

3. In-House-Built Ultra-Broadband Photonic SFMCW Radar

To generate ISAR images, SFMCW photonic radar demonstrates superior performance over Linear Frequency Modulated Continuous Wave (LFMCW) radar for ISAR imaging. SFMCW radar offers a fast processing system with enhanced range resolution, improved Signal-To-Noise Ratio (SNR), reduced Doppler ambiguity, flexible frequency step design, better clutter suppression, simplified hardware implementation, and easier calibration [19]. These advantages make photonic SFMCW radar particularly well-suited for achieving high down-range and cross-range resolution in the accurate ISAR imaging of LSS targets. Due to the inverse relationship between range resolution and bandwidth, as well as between cross-range resolution and look-angle width, achieving better-resolved ISAR images in both the range and cross-range domains necessitates the use of wide frequency bandwidths and large angular apertures [20].

An ultra-broadband SFMCW photonic radar system has been designed and developed in an RF-photonic laboratory, capable of operating across a wide instantaneous bandwidth ranging from 6 to 12 GHz. This system is specifically tailored for collecting backscattered signals from various LSS aerial targets, considering variations in frequency and look-angle. The system architecture, illustrated in Figure 3, consists of a Transmission (Tx) module, a Reception (Rx) module, an Analog-to-Digital Converter (ADC), and a data processing unit.

The radar system initiates signal generation at an Intermediate Frequency (IF) range of $1.5 - 3$ GHz using a Step-Frequency Continuous Wave (SFCW) Direct Digital Synthesizer (DDS), controlled via a Digital Signal Processing (DSP) unit. The generated RF signal is split into in-phase (I)

and Quadrature phase (Q) components by using a 90° hybrid coupler and subsequently fed to a Dual-Parallel Mach Zehnder Modulator (DPMZM), which modulates an optical carrier signal at 1550 nm. Through a proper biasing of the two sub-MZMs at their maximum transmission points, predominantly generates the even-order optical sidebands, and the third MZM is kept at a minimum biasing point to eliminate the optical carrier, ensuring that only ± 2nd-order sidebands remain [21]. After the modulation process, the optical signal is split via a 3 dB Optical Coupler (OC), where, at the upper arm, the signal is amplified by using an Erbium-Doped Fiber Amplifier (EDFA) and then converted back to the electrical domain through a Photodetector (PD1).

The resulting electrical signal generates a frequency-quadrupled SFMCW waveform in the 6-12 GHz range. Then the RF signal is further amplified via a Power Amplifier (PA) and transmitted to the free space using a Vivaldi horn antenna. The backscattered signals at multiple frequencies and look angles are received at a uniform sampling rate.

To enhance the weak received signal, a Low-Noise Amplifier (LNA) is used before routing the signal to a Phase Modulator (PM-MZM), where it modulates the phase of the Local Oscillator (LO) signal. After that, an Optical Bandpass Filter (OBPF) is used to extract the desired 1st-order optical sidebands, which are subsequently detected by another Photodetector (PD2). To suppress the high-frequency noise and amplify the base-band signal, a Low-Pass Filter (LPF) and A Base-Band Amplifier (BBA) are employed. Finally, the resultant IF signal is digitized through an ADC and processed in a MATLAB environment for the ISAR image construction, dataset preparation, and classification using the proposed DCNN model.

4. 2D-ISAR Imaging and Dataset Formulation Methodology

In the MATLAB environment, a modified ISAR imaging algorithm is applied to generate the 2-D ISAR images of the LSS targets and further to classify accurately using a DCNN model. The backscattered data are collected by the developed radar at multiple frequencies and look angles and then processed through a 2-D inverse Fourier transform using the following Eq. to generate the ISAR image.

$$ISAR(r, cr) = \iint E^s(f, \phi) \cdot e^{jk_x r} \cdot e^{jk_y cr}\, dk_x\, dk_y \quad (1)$$

Where,

$$kx = \frac{4\pi f}{c}\ cos\phi \cong \frac{4\pi f}{c}\ and$$

$$ky = \frac{4\pi f}{c}\ sin\phi \cong \frac{4\pi f}{c}\ \phi \quad (2)$$

Here, r, cr, f, and ϕ denote the down-range, cross-range, frequency, and azimuth angle increment, respectively. The backscattered data Es depends on both frequency and angle variations, where c represents the speed of light. However, the data are uniformly sampled in frequency and angle (ω–Ω) domain, and after that, a polar reformatting is applied to interpolate the data onto a uniform kx-ky grid. After the interpolation, a 2-D Hamming window is applied to reduce the image sidelobes, and then a 2-D Inverse Fast Fourier Transform (IFFT) is performed to generate the ISAR images.

In this work, ISAR images were chosen due to their ability to support extensive feature extraction through CNN, therefore enhancing the classification accuracy [22]. To ensure the diversity of the dataset, the target was positioned on a turntable, which was controlled by a remote control along the variation of yaw, roll, and pitch axes (as shown in Figure 2). The implemented angular adjustment is mentioned in Table 1.

The dataset was generated through a completely controlled experimental trial, capturing the backscattered radar signals from the targets at various ranges and orientations. These orientations were carefully chosen to replicate real-world flight and hovering conditions, ensuring practical scenarios like LSS targets cannot sustain flight at extreme angles (e.g., near 90◦). Similarly, the pitch and roll angle ranges were considered to reflect realistic airborne maneuvers. In this experiment, the pitch and roll axes were varied within a range of −20° to +20 ° with an incremental resolution of 5°, while the yaw angle spanned from −100° to +100° at the same incremental resolution. Therefore, for each experimental trial, a total of 9 distinct pitch angles were combined with 40 yaw orientations, resulting in 40 × 9 = 360 unique look angles. Similarly, for 9 different roll angles, each combined with 40 different yaw angles, resulted in another set of 40 × 9 = 360 orientations. Thus, in this process, a total of [360+360] = 720 distinct samples per class were generated for the first five target classes, which were further processed to generate 3-color channel images corresponding to each class.

In addition, with the single-target experiment, a combined class (sixth class) were introduced insuring the combined scenario of two LSS targets: a bionic-bird and a mini-helicopter For these combined operation two cases were considered: 1) The bionic-bird was kept stationary while the mini helicopter was rotated along the yaw axis from−100° to +100° at 5° resolution creating total 40 distinct angles and along the pitch axis from −20° to + 20° at 5° resolution creates 9 distinct angles, resulting to a total of 40×9=360 unique orientations and generating a [360×3] 3-color channel images for the dataset. 2) Similarly, the mini-helicopter was kept static while the bionic bird was subjected to rotation at the same yaw and pitch variations, producing [360 × 3] 3-color channel imag

Table 1. Characteristics of LSS target classes with different angular and range orientations

Class Name	Targets physical parameters	Aspect angle of operation			Range of operation	No. of org., samples	Augmented samples
		Yaw	Pitch	Roll			
RC plane	Number of wings: 02 Length of wing: 54 cm Length of target: 110 cm 2-blade propeller; length: 7 cm Weight:1200 g	-100° to +100° @ 5° res., [40 diff., look angles]	-20° to +20° @ 5° res., [9 diff., look angles]	-20° to +20° @ 5° res., [9 diff., look angles]	(5-15) m	[40×9 + 40×9]= [720×3]	[1000×3]
Mini-helicopter	Number of wings: 02 Length of wing: 45 cm Length of target: 85 cm Secondary wing length: 20 cm Weight: 900 g				(5-10) m	[40×9 + 40×9]= [720×3]	[1000×3]
DJIF450 (2-blade propeller system)	Propeller blade: 02 Blade length: 14 cm Arm length: 16 cm Weight: 800 g				(5-15) m	[40×9 + 40×9]= [720×3]	[1000×3]
Scythe 4s racer (3-blade propeller system)	Propeller blade: 03 Blade length: 6 cm Arm length: 9 cm Weight: 250 g					[40×9 + 40×9]= [720×3]	[1000×3]
Bionic Bird	Number of wings: 02 Length of wing: 10 cm Length of bird: 19 cm Weight: 63 g				(5-10) m	[40×9 + 40×9]= [720×3]	[1000×3]
A combination of a bionic bird & a mini-helicopter	Bionic Bird + Mini-helicopter: bionic-bird is static, while the mini-helicopter is	rotated in yaw axis -100° to +100° @ 5° res., [40 diff., look angles]	rotated in the pitch axis -20° to +20° @ 5° res., [9 diff., look angles]	-		[40×9]= [360×3]	[1000×3]
	Bionic Bird + Mini-helicopter: the mini-helicopter is static, while the bionic bird is	rotated in yaw axis -100° to +100° @ 5° res., [40 diff., look angles]	rotated in the pitch axis -20° to +20° @ 5° res., [9 diff., look angles]	-		[40×9]= [360×3]	[1000×3]

Thus, a highly diversified dataset was developed under systematic and controlled experimental conditions to ensure the realistic target orientation, which enhances the robustness of the proposed Deep Convolutional Neural Network (DCNN) architecture for accurate classification and identification of LSS aerial targets in real-world operational environments. For balancing the computational efficiency and feature preservation, the resolution of the images is considered as 224×224×3, where a scaling factor 1/255 is applied to normalize the pixel values to the [0,1] range. It helps to stabilize the training and enhances the convergence by preventing a large gradient update, keeping consistency in data processing. After conducting several trial-and-error experiments, it was determined that this dimension should be fixed to achieve maximum accuracy while minimizing size. Finally, standard data augmentation methods-such as rotations of 30° and 60°, as well as horizontal flipping (mirroring the rows and columns)-are applied to the images to create multiple variations of the original dataset before feeding them into the convolutional base module during training. Thus, this comprehensive approach resulted in a dataset of ISAR images captured from the radar, creating a small-scale dataset of [4320 × 3] samples, named the “DIAT

ISAR-sATIs" dataset. Further, by augmentation, this dataset is converted into a large-scale dataset of 6000 samples for accurate CNN-based classification of the LSS targets. Used the tensorflow library of ImageDataGenerator to augment the data. The "DIAT-ISAR-sATIs" dataset was divided into training, validation, and testing sets in a 70%:15%:15% ratio.

5. Post-Processing of Photonics Radar-Generated ISAR Images

The ISAR images generated by the proposed photonic SFMCW radar system often suffer from considerable noise and blur, making them unsuitable for direct use in DCNN for target classification. In [17], a post-processing step is discussed to extract the contour of an image by improving the critical features and reducing the background artifacts, which can be used to improve the ISAR image quality. According to their method, a modified Smallest Univalue Segment Assimilating Nucleus (SUSAN) edge detection algorithm will be applied to the ISAR image to enhance structural clarity by reducing background noise. Note that, here, for the local neighborhood analysis, a circular mask of 37 pixels with a radius of 3 is considered. Thus, a global mean intensity of the image is used to calculate an adaptive threshold t, which can be provided by,

$$t = k.\frac{1}{MN}\sum_{i=1}^{M}\sum_{j=1}^{N} im(i,j) \tag{3}$$

Here, the object-to-image size ratio is considered as the scaling factor by k, and by adding a geometrical threshold, the SUSAN response function is further altered to increase its resilience to noise.

$$G = \frac{3n_{max}}{4} \tag{4}$$

Where n_{max} is the highest value of the mask's similarity sum S, which can be calculated as,

$$\mathrm{S} = \sum_{i \in USAN} \mathrm{C}(\mathrm{Pi}, \mathrm{P0}) \tag{5}$$

And in the above Eq., C represents the pixel's brightness within the USAN region, considering a nucleus (central point) can be computed as,

$$C(Pi, P0) = exp\left(-\left(\frac{im(x_i, y_i) - im(x_0, y_0)}{t}\right)^6\right) \tag{6}$$

The decision rule for each pixel P_0 is defined as:

$$R(P0) = \begin{cases} G - S, & if\ S < G \\ im(x_0, y_0), & if\ im(x_0, y_0) > t \\ 0, & otherwise \end{cases} \tag{7}$$

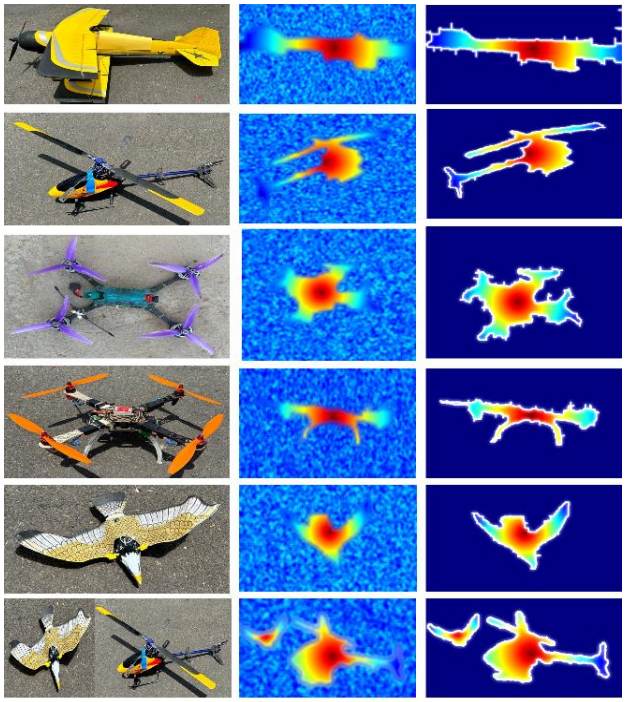

(a) Real LSS target images (b) ISAR image generated from the radar (c) After image processing ISAR image

Fig. 4 Post image processing on ISAR images of LSS targets

The result of the SUSAN operation serves as the input to a Variational Level Set (VLS) method, which is applied to refine the target shape by evolving a contour that best captures object boundaries. This integrated method yields a noise-suppressed, contour-based ISAR image I′, which preserves discriminative target features essential for reliable classification. The outcome of the post-processing stage is illustrated in Figure 4.

6. Proposed DCNN Architecture and its Implementation

This section presents the design of the proposed DCNN multi-class classification architecture along with details of its implementation platform.

6.1. Design of a Proposed DCNN Architecture

In order to propose/design an appropriate DCNN model for the classification of LSS targets (i.e., six classes) based on their 2D-ISAR images, the most recently (last decade) developed and most relevant pre-trained DCNN models: "VGG16 (2014)", "VGG19 (2014)", "ResNet50 (2016)", "Efficient NetB0 (2019)", "InceptionV3 (2016)", "DenseNet121 (2017)", & "MobileNetV2 (2018)" are considered in this work. By applying the 2D-ISAR dataset, i.e., "DIAT-ISAR sATIs" directly into the considered DCNN models will overfit them due to their inherent complexity (i.e., huge layers/ FLOPS/ memory/ parameters) nature, and it will result in poor classification accuracy.

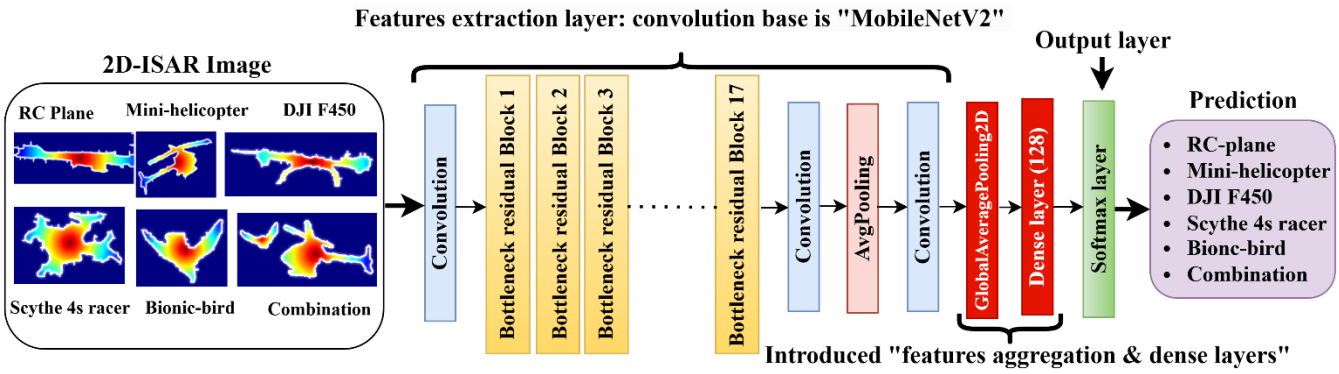

Fig. 5 A Proposed DCNN Architecture: Fine-tuned MobileNetV2 Model

Table 2. Specifications of Pretrained DCNN Models: Original Vs. Modified Versions

DCNN Model	Original				Modified			
	FLOPs	Layers	Memory (MB)	Param	FLOPs	Layers	Memory (MB)	Param
VGG16	15,369,313,554	23	105.15	27,563,334	15,356,544,594	20	56.39	14,781,638
VGG19	19,531,763,986	26	125.40	32,873,030	19,522,168,498	24	76.65	20,090,822
ResNet50	3,866,982,840	177	97.80	25,636,712	3,865,194,834	180	90.98	23,850,758
EfficientNetB0	394,874,867	240	20.34	5,330,564	393,756,557	232	16.08	4,214,313
InceptionV3	5,725,484,312	48	90.99	23,851,784	2,842,249,602	50	84.17	22,065,830
DenseNet121	2,835,444,152	121	30.76	8,062,504	2,834,549,074	123	27.35	7,169,478
MobileNetV2	300,000,000	155	15.00	5,330,571	299,798,514	157	9.24	2,422,726

Therefore, it is essential to modify the considered DCNN models to the greatest extent possible, aiming to reduce complexity and achieve the maximum possible classification accuracy. In this work, the required modifications to the considered DCNN models are made by replacing their "flatten layer" with a "Global Average Pooling (GAP) layer" and a "dense layer" between the feature extraction layer and the output layer, as shown in Figure 5.

In all the considered models, the feature extraction base is frozen, i.e., the weights of it are kept as they are. In this proposed modification approach, the introduction of a "GAP layer" aggregates all the features from the previous "features extraction layer" while the "dense layer" enables the network to adapt the pre-trained features to a new task, which is necessary because the model was originally trained with/ for different images. That means the "dense layer" helps tailor the model to the specifics of the new data set and problem [23]. The complexity is significantly reduced by the proposed approach, and the statistics associated with it are given in Table 2. Among all the modified DCNN models, to investigate which one is most suitable for the intended classification problem, 70% of the dataset ("DIAT-ISAR-sATIs") is used to train all the modified DCNN models.

All the models are optimized using the adaptive moment estimation optimizer. For training, an initial learning rate of 0.01 was used for the first 10 epochs, then increased to 0.02 for the next 5 epochs, reduced to 0.001 for the following 10 epochs, and set to 0.0001 for the remaining epochs, with a momentum of 0.9. The network is trained with a batch size of 16 and a maximum of 35 epochs.

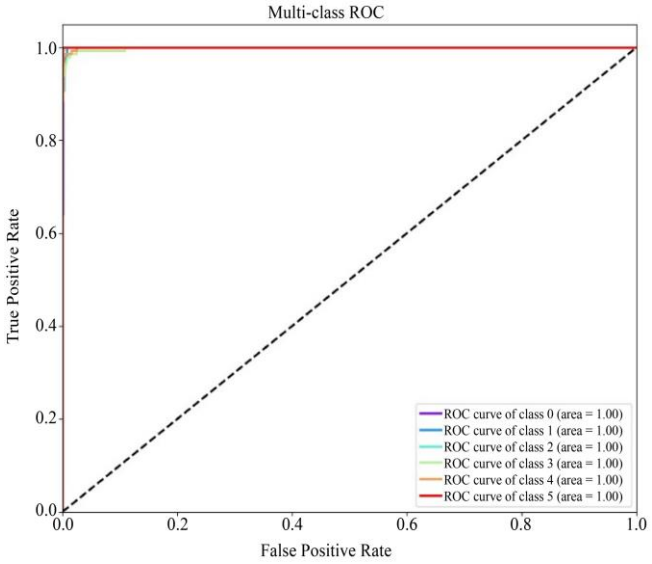

Fig. 6 The ROC curve for the proposed DCNN model on the validation test dataset, with an AUC of 1.0 for all the targets

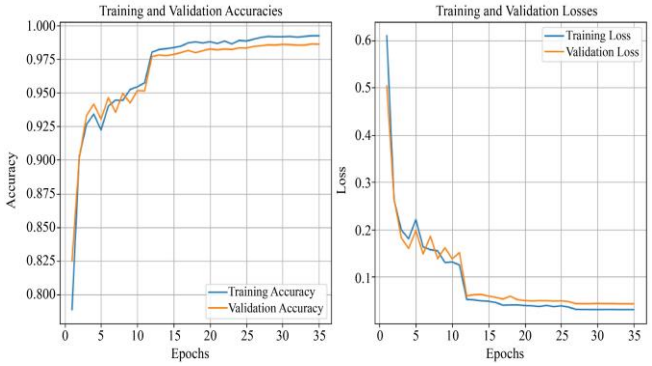

Fig. 7 The categorical accuracy (left) and cross-entropy loss (right) plots for the proposed DCNN model

The categorical cross-entropy loss function was employed for training the model. The remaining 15% dataset, of dimension [150 × 6 × 3], is used for testing the modified/ trained DCNN models.

6.2. Implementation Platform

The design, testing, performance validation experiments and final implementation of the proposed DCNN model i.e., "MobileNetV2" based convolution base classifier are accomplished /conducted in a workstation equipped with 256 GB of memory, an NVIDIA Quadro RTX 6000 GPU with 24.0 GB of memory, an Intel Xeon Gold 6140 Processor running at 2.30 GHz, CUDA Toolkit version10.0.130, and Cu DNN version 7.6.0.

6.3. Results and Data Analysis

The experimental results associated with the design characterization of the proposed DCNN model, as well as its classification performance on validation and open-field samples, are reported and analyzed in this section.

Table 3. Classification Report of the Proposed DCNN Model on the Validation Test Dataset of "DIAT-ISAR-sATIs"

Target Classes	Precision	Recall	F1-Score
RC plane	0.98	0.97	0.97
Mini-helicopter	0.99	0.99	0.99
DJI F450	0.96	0.97	0.97
Scythe 4s racer	1.00	1.00	1.00
Bionic-bird	0.99	0.99	0.99
Combination	1.00	1.00	1.00
Accuracy	—	—	98.67
Macro Avg	0.99	0.99	0.99
Weighted Avg	0.99	0.99	0.99

6.4. Design Characterization of Proposed DCNN Model

The statistical analysis/ evaluation related to the design characterization of the proposed DCNN architecture is performed using standard performance measurement metrics, i.e., precision, recall, and F1-score. Moreover, this study reports accuracy, macro average, and weighted average to provide a more comprehensive evaluation of the proposed DCNN models, with the corresponding statistical results presented in Table 3. As shown, the proposed DCNN model achieves an overall classification accuracy of 98.67% on the validation dataset, with precision, recall, and F1-score exceeding 96% across all six LSS target classes. These results demonstrate the model's effectiveness in class-wise classification of LSS targets. To further illustrate its performance, the Receiver Operating Characteristic (ROC) curves were generated to show the trade-off between specificity and sensitivity for each class, as presented in Figure 7. The curves are all close to the top-left corner, indicating high specificity and sensitivity. Additionally, the model achieves an Area Under the Curve (AUC) of 1.0 for all targets, confirming its strong capability in distinguishing the six aerial LSS targets. The categorical accuracy (left one) and cross-entropy loss (right one) plots are also generated, shown in Figure 7, and as therein, they indicate that the model neither over-fits nor under-fits when using the DCNN model on the test dataset.

6.5. Experiments for Classification Accuracy Analysis

The classification accuracy results of the proposed DCNN model on both the validation dataset and the open-field new/unknown dataset are as follows:

6.5.1. Validation Experiments

The reserved validation dataset [150 × 6 × 3], i.e., 15% of "DIAT-ISAR-sATIs", is applied to the proposed DCNN model, and the confusion matrices demonstrating the class-wise classification accuracy are shown in Figure 8, which gives the minimal false-negative and false positive with the overall classification accuracy of ≈ 0.99 (98.67%), at the

misclassification rate of ≈ 0.01 (1.33%)). Moreover, these validation test results prove the LSS targets classification performance effectiveness of the proposed DCNN model.

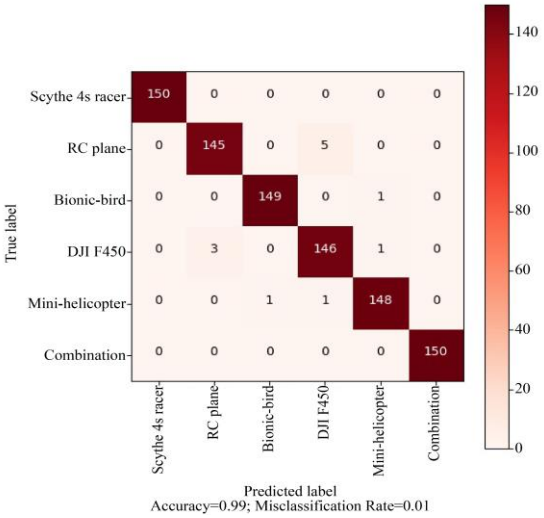

Fig. 8 Confusion matrix of the proposed DCNN model on the validation dataset

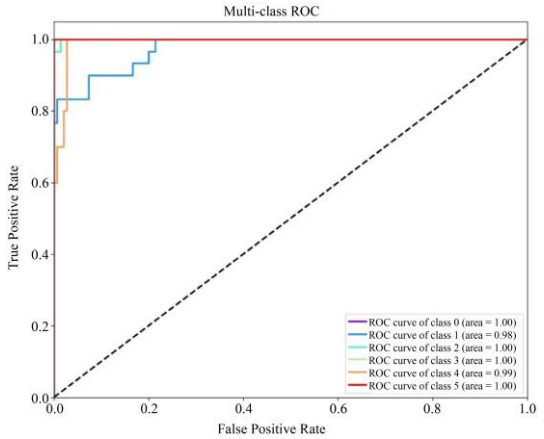

Fig. 9 The ROC curve for the proposed DCNN model on the open-field dataset, with an AUC of ≥ 0.98 for all the targets

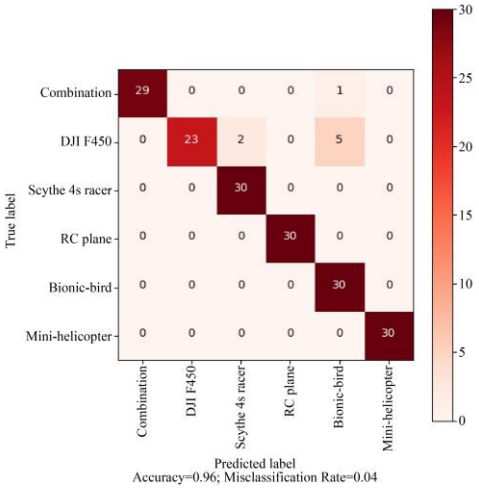

Fig. 10 Confusion matrix of the proposed DCNN model on the open-field dataset

6.5.2. Open-Field Classifications

To further evaluate the classification performance of the proposed DCNN model, a new dataset was collected to test its ability on a more diverse set of 2D-ISAR images. For this purpose, the LSS targets shown in Figure 1 were operated in various postures and orientations in an open-field environment in front of the developed photonic radar, resulting in a newly formulated dataset of dimensions [30 × 6 × 3]. This dataset is entirely unknown to the DCNN model, as it is based on instantaneously collected ω–Ω data.

The new dataset was then fed into the trained DCNN model, and the classification performance metrics were calculated, with the results presented in Table 4 and Figures 9 and 10. As shown in Table 4, the proposed DCNN model achieves an overall classification accuracy of 95.56% on this newly collected dataset, with precision, recall, and F1-score exceeding 96% for all six LSS target classes. The corresponding ROC plot, shown in Figure 9, gives the AUC at 0.98 for all the LSS targets' classes, which witnesses the drop in the classification accuracy of the proposed DCNN model. The respective confusion matrix for this open-field experiment is shown in Figure 10, in which the overall classification accuracy is ≈ 0.96 (95.56%) at a misclassification rate of ≈ 0.04 (4.44%). Thus, the proposed DCNN model gives relatively low true positive cases and high false positive cases.

The main reason for the drop in classification accuracy is that the feature extraction kernel, i.e., the convolutional base in the proposed DCNN model, was not originally designed/weighted for the "DIAT-ISAR sATIs" dataset. Therefore, creating/designing a new lightweight DCNN model/ architecture from scratch, incorporating the FLOPs, layers, memory, and parameters optimization at all the stages/levels, aiming at an increased classification accuracy, is only the appropriate way forward to successfully address the requirement of accurate classification of LSS targets, which is one of the near-future research works.

Table 4. Classification Report of the Model Using Pre-trained MobileNetV2 on the DIAT-ISAR-sATIs Open Field Test Dataset

Target Classes	Precision	Recall	F1-Score
RC plane	1.00	1.00	1.00
Mini-helicopter	1.00	1.00	1.00
DJI F450	1.00	0.77	0.87
Scythe 4s racer	0.94	1.00	0.97
Bionic-bird	0.83	1.00	0.91
Combination	1.00	0.97	0.98
Accuracy	—	—	95.56
Macro Avg	0.96	0.95	0.95
Weighted Avg	0.96	0.95	0.95

Table 5. Classification Accuracy of Pre-trained DCNN Models on DIAT-ISAR-sATIs Validation and Open Field Test Datasets

DCNN Models	Validation Test (%)	Open Field Test (%)
VGG16	97.22	95.56
VGG19	97.00	93.89
ResNet50	82.33	83.89
EfficientNetB0	23.44	71.59
InceptionV3	97.22	96.35
DenseNet-121	97.89	93.42
MobileNetV2	**98.67**	**95.56**

6.5.3. Performance Analysis of Pre-Trained DCNN Models

Table 5 presents the classification accuracy of several pre-trained DCNN models on the DIAT-ISAR-sATIs validation dataset and a real-world Open Field Test dataset. Among all the evaluated models, MobileNetV2 achieved the highest validation accuracy of 98.67%, demonstrating its superior ability to learn discriminative features from the DIAT-ISAR sATIs dataset. It also maintained strong generalization with a 95.56 % accuracy on the Open Field Test dataset, matching the performance of VGG 16 and closely trailing InceptionV3 (96.35%).

Due to the higher accuracy and computational efficiency, MobileNetV2 is a great option for real-time and embedded applications with a limited source. Due to its lightweight design, MobileNetV2 not only outperformed the minimum accuracy but also provided faster inference compared to other deeper models, such as ResNet 50 and DenseNet-121.

The result analysis shows that, even though a number of other models perform well in controlled validation settings, MobileNetV2 provides constant high accuracy in both the controlled and real-world environment, which proves the robustness and suitability for deployment in practical scenarios where reliable classification is essential.

6.5.4. Comparative Performance Analysis with Existing Methods

Table 6 presents a comparative evaluation of the proposed ne-tuned MobileNetV2 model against several existing deep learning-based methods, including a Hybrid Transformer [24], conventional deep learning classifiers [25], sparse autoencoders [26], and a pre-trained VGG16 model [12]. The performance is assessed on both the validation and open field test sets of the DIAT-ISAR-sATIs dataset. Among all the models, the proposed fine-tuned MobileNetV2 achieves the highest classification accuracy of 98.67% on the validation set and 95.56% on the open eld test set. In contrast, the other methods exhibit lower performance, particularly under open field test conditions, indicating reduced generalization capability in real-world scenarios.

Table 6. Classification accuracy of existing deep learning models and the proposed model on the DIAT-ISAR-sATIs Validation and Open Field Test datasets

Methods	Validation Test (%)	Open Field Test (%)
Hybrid Transformer [24]	96.25	92.34
Deep learning classifier [25]	94.10	90.12
Sparse autoencoder [26]	90.22	87.53
Pre-trained VGG16 [12]	92.45	88.90
Fine-tuned MobileNetV2 (Proposed)	**98.67**	**95.56**

However, both the VGG16 and MobileNetV2 are originally pre-trained on large-scale datasets such as ImageNet; their approaches to use are very different. The VGG16 model is a fixed feature extractor without any further adaptation to the target domain. In contrast, the proposed model leverages transfer learning by fine-tuning all layers of MobileNetV2 on the radar-based DIAT-ISAR-sATIs dataset. Thus, the network can be fully adapted by its feature representation to the radar spectrograms and human activity.

Effective feature extraction with less computational overhead is made possible by MobileNetV2's efficient architecture, which includes depthwise separable convolutions and inverted residual connections. When combined with end-to-end fine-tuning and a lightweight classification head, the model becomes highly capable of capturing subtle spatial and temporal variations in the radar signals. These properties make the proposed method not only superior in controlled validation settings but also robust under operational open field conditions, establishing it as a strong candidate for real-time radar-based human activity recognition.

7. Conclusion

This study introduces the DIAT-ISAR-sATIs dataset, which comprises 6,000 high-resolution ISAR images of Low, Small, and Slow (LSS) aerial targets. To demonstrate the effectiveness of the dataset for radar-based target recognition, a transfer learning-based Deep Convolutional Neural Network (DCNN) model was proposed using the MobileNetV2 architecture. The model includes all layers of the original MobileNetV2 backbone, followed by a Global Average Pooling layer and a task-specific Dense and Softmax classification head. The proposed fine-tuned MobileNetV2 achieved an accuracy of 98.67% on the validation set and 95.56% on the open-field test set, outperforming other existing deep learning methods. The model also demonstrated robust performance in challenging scenarios involving multiple targets, indicating strong generalization capabilities. The DIAT-ISAR-sATIs dataset was carefully curated to include variations in operational parameters such

as range, aspect angle, and target geometry, ensuring a diverse and representative sample of real-world aerial LSS targets. To benchmark its effectiveness, several state-of-the-art models, including Hybrid Transformer, Sparse Autoencoder, and VGG16, were evaluated. Results show that the fine-tuned MobileNetV2 offers superior performance due to its efficient design and ability to learn domain-specific features through transfer learning. Future work will focus on designing a novel lightweight DCNN architecture optimized for real-time, on-device deployment, making it suitable for edge-based aerial target recognition systems.

References

[1] Samedh Sachin Kari, A. Arockia Bazil Raj, and K. Balasubramanian, "Evolutionary Developments of Today's Remote Sensing Radar Technology-Right From the Telemobiloscope: A Review," *IEEE Geoscience and Remote Sensing Magazine*, vol. 12, no. 1, pp. 67-107, 2023. [CrossRef] [Google Scholar] [Publisher Link]

[2] Hossein Emami et al., "Simultaneous Echo Power and Doppler Frequency Measurement System Based on Microwave Photonics Technology," *IEEE Transactions on Instrumentation and Measurement*, vol. 66, no. 3, pp. 508-513, 2017. [CrossRef] [Google Scholar] [Publisher Link]

[3] Bir Bhanu, "Automatic Target Recognition: State of the Art Survey," *IEEE Transactions on Aerospace and Electronic Systems*, vol. AES-22, no. 4, pp. 364-379, 1986. [CrossRef] [Google Scholar] [Publisher Link]

[4] Massimiliano Pieraccini, Lapo Miccinesi, and Neda Rojhani, "RCS Measurements and ISAR Images of Small UAVs," *IEEE Aerospace and Electronic Systems Magazine*, vol. 32, no. 9, pp. 28-32, 2017. [CrossRef] [Google Scholar] [Publisher Link]

[5] Sampurna De, and A.A. Bazil Raj, "A Survey on Photonics Technologies for Radar Applications," *Journal of Optics*, vol. 52, pp. 90-119, 2023. [CrossRef] [Google Scholar] [Publisher Link]

[6] Andrea Manno-Kovacs et al., "Image Based Robust Target Classification for Passive ISAR," *IEEE Sensors Journal*, vol. 19, no. 1, pp. 268-276, 2018. [CrossRef] [Google Scholar] [Publisher Link]

[7] Hari Kishan Kondaveeti, and Valli Kumari Vatsavayi, "Abridged Shape Matrix Representation for the Recognition of Aircraft Targets from 2D ISAR Imagery," *Advances in Computational Sciences and Technology*, vol. 10, no. 5, pp. 1103-1122, 2017. [Google Scholar] [Publisher Link]

[8] Yann LeCun, Yoshua Bengio, and Geoffrey Hinton, "Deep Learning," *Nature*, vol. 521, pp. 436-444, 2015. [CrossRef] [Google Scholar] [Publisher Link]

[9] Xueru Bai et al., "REMI: Few-Shot ISAR Target Classification via Robust Embedding and Manifold Inference," *IEEE Transactions on Neural Networks and Learning Systems*, vol. 36, no. 4, pp. 6000- 6013, 2025. [CrossRef] [Google Scholar] [Publisher Link]

[10] Chow Yii Pui et al., "Target Classification for 3D-ISAR Using CNNs," *IEEE Transactions on Aerospace and Electronic Systems*, vol. 60, pp. 94-105, 2024. [CrossRef] [Google Scholar] [Publisher Link]

[11] A. Lazarov, and C. Minchev, "ISAR Image Recognition Algorithm and Neural Network Implementation," *Cybernetics and Information Technologies*, vol. 17, no. 4, pp. 183-199, 2017. [Google Scholar] [Publisher Link]

[12] Harish C. Kumawat et al., "DIAT-μSAT: Small Aerial Targets' Micro-Doppler Signatures and Their Classification Using CNN," *IEEE Geoscience and Remote Sensing Letters*, vol. 19, pp. 1-5, 2021. [CrossRef] [Google Scholar] [Publisher Link]

[13] Dongsuk Park et al., "Radar-Spectrogram-Based UAV Classification Using Convolutional Neural Networks," *Sensors*, vol. 21, no. 1, pp. 1-18, 2021. [CrossRef] [Google Scholar] [Publisher Link]

[14] Neeraj Pandey, and Shobha Sundar Ram, "Classification of Automotive Targets Using Inverse Synthetic Aperture Radar Images," *IEEE Transactions on Intelligent Vehicles*, vol. 7, no. 3, pp. 675-689, 2022. [CrossRef] [Google Scholar] [Publisher Link]

[15] Arthur Holland Michel, "*Counter-Drone Systems*," Center for the Study of the Drone at Bard College, Report, pp. 1-23, 2018. [Google Scholar] [Publisher Link]

[16] Ian Goodfellow, Yoshua Bengio, and Aaron Courville, *Deep Learning*, MIT Press, pp. 1-775, 2016. [Google Scholar] [Publisher Link]

[17] M.N. Saidi et al., "Aircraft Target Recognition: A Novel Approach for Features Extraction from ISAR Images," *2009 International Radar Conference "Surveillance for a Safer World" (RADAR 2009)*, Bordeaux, France, pp. 1-5, 2009. [Google Scholar] [Publisher Link]

[18] José Capmanyet al., "Microwave Photonics: Current Challenges towards Widespread Application," *Optics Express*, vol. 21, no. 9, pp. 22862-22867, 2018. [CrossRef] [Google Scholar] [Publisher Link]

[19] Caner Ozdemir, *Inverse Synthetic Aperture Radar Imaging With MATLAB Algorithms*, 2nd ed., General & Introductory Electrical & Electronics Engineering, John Wiley & Sons, pp. 1-672, 2021. [Google Scholar] [Publisher Link]

[20] Donald R. Wehner, *High-Resolution Radar*, 2nd ed., Artech House, Boston, pp. 1-593, 1994. [Google Scholar] [Publisher Link]

[21] Chun-Ting Lin et al., "Optical Millimeter-Wave Signal Generation Using Frequency Quadrupling Technique and No Optical Filtering," *IEEE Photonics Technology Letters*, vol. 20, no. 12, pp. 1027-1029, 2008. [CrossRef] [Google Scholar] [Publisher Link]

[22] Valli Kumari Vatsavayi, and Hari Kishan Kondaveeti, "Efficient ISAR Image Classification Using MECSM Representation," *Journal of King Saud University - Computer and Information Sciences*, vol. 30, no. 3, pp. 356-372, 2018. [CrossRef] [Google Scholar] [Publisher Link]

[23] P. Anantha Prabha, G. Suchitra, and R. Saravanan, "Cephalopods Classification Using Fine Tuned Lightweight Transfer Learning Models," *Intelligent Automation & Soft Computing*, vol. 35, no. 3, pp. 3065-3079, 2023. [CrossRef] [Google Scholar] [Publisher Link]

[24] Ruihang Xue et al., "Sequential ISAR Target Classification Based on Hybrid Transformer," *IEEE Transactions on Geoscience and Remote Sensing*, vol. 60, pp. 1-11, 2022. [CrossRef] [Google Scholar] [Publisher Link]

[25] Soyoon Park et al., "Classification of ISAR Images Generated from Model-based Approaches Using Deep Learning," *2025 International Conference on Information Networking (ICOIN)*, Chiang Mai, Thailand, pp. 312-316, 2025. [CrossRef] [Google Scholar] [Publisher Link]

[26] Xingyu He, Ningning Tong, and Xiaowei Hu, "Automatic Recognition of ISAR Images Based on Deep Learning," *2016 CIE International Conference on Radar (RADAR)*, Guangzhou, China, pp. 1-4, 2016. [CrossRef] [Google Scholar] [Publisher Link]